

Band structure reconstruction across nematic order in high quality FeSe single crystal as revealed by optical spectroscopy study

Haipeng Wang,¹ Zirong Ye,² Yan Zhang,^{2,3} and Nanlin Wang^{2,3,*}

¹*Beijing National Laboratory for Condensed Matter Physics,*

Institute of Physics, Chinese Academy of Sciences, Beijing 100190, China

²*International Center for Quantum Materials, School of Physics, Peking University, Beijing 100871, China*

³*Collaborative Innovation Center of Quantum Matter, Beijing 100871, China*

We perform an in-plane optical spectroscopy measurement on high quality FeSe single crystals grown by a vapor transport technique. Below the structural transition at $T_s \sim 90$ K, the reflectivity spectrum clearly shows a gradual suppression around 400 cm^{-1} and the conductivity spectrum shows a peak at higher frequency. The energy scale of this gap-like feature is comparable to the width of the band splitting observed by ARPES. The low-frequency conductivity consists of two Drude components and the overall plasma frequency is smaller than that of the FeAs based compounds, suggesting a lower carrier density or stronger correlation effect. The plasma frequency becomes even smaller below T_s which agrees with the very small Fermi energy estimated by other experiments. Similar to iron pnictides, a clear temperature-induced spectral weight transfer is observed for FeSe, being indicative of strong correlation effect.

Keywords: Iron-based superconductor, Optical spectroscopy, Nematic phase, Band reconstruction

I. INTRODUCTION

The PbO-type FeSe has the simplest structure in iron-based superconductors with a stack of edge-sharing FeSe₄-tetrahedra layer by layer. The undoped FeSe exhibits superconducting transition at $T_c \sim 9$ K, but it can easily reach 37 K upon applying hydrostatic pressure¹ and over 40 K by intercalating space layers^{2,3}. The T_c of the single layer FeSe film grown on SrTiO₃ (STO) has been reported to be $\sim 60\text{--}70$ K in angle-resolved photoemission spectroscopy (ARPES) experiments⁴⁻⁷ and Meissner effect measurements^{8,9}. A recent in-situ transport measurement on monolayer of FeSe grown on SrTiO₃ even shows a sign of superconductivity over 100 K¹⁰.

FeSe undergoes a structural transition at $T_s = 90$ K. However, different from the iron arsenic based systems, in which a tetragonal to orthorhombic structural transition usually precedes or coincides with stripe-type antiferromagnetic (AFM) order, there is no long-range magnetic order at any temperature in FeSe^{11,12}. Experimental and theoretical studies suggested that the structural transition is caused by the electronic nematicity which breaks the C_4 rotational symmetry. It is widely believed that the mechanism of nematicity is tied to the pairing mechanism of high- T_c superconductivity in Fe-based superconductors. However, whether the nematicity has a spin or orbital origin remains controversial. On the other hand, FeSe superconductors also show several other peculiar physical properties. A recent study shows that FeSe has extremely small Fermi energy (ε_F) and the superconducting energy gap (Δ) is comparable to the Fermi energy. This places FeSe superconductor in the Bose-Einstein condensation - Bardeen-Cooper-Schrieffer (BEC-BCS) crossover regime¹³. An ARPES study¹⁴ revealed the existence of Dirac cone band dispersions in FeSe thin films, and an theoretical study¹⁵ predicated a

nematicity-driven topological phase transition in FeSe. In any sense, the nature of these fascinating phenomena and their interplay need to be understood comprehensively by using different experimental methods.

For a long time, the single crystal growth of FeSe with a pure ab-plane facet turned out to be difficult because of the narrow phase formation range. The reported plate-like single crystals grown by flux method usually contained secondary phase and quite often had a (101) surface¹⁶, making it very difficult to study the intrinsic in-plane properties. As a result, pure FeSe was far less studied than other Fe-based superconductors, particularly by spectroscopic techniques. Although some efforts were made in growing relatively thick ab-plane thin-films by pulsed laser deposition technique, which permitted measurement of some in-plane properties, e.g. by optical spectroscopy technique, the quality of the films grown by this technique was far from perfect. A substantial progress was made only after the vapor transport growth technique was used to grow FeSe crystals¹⁷. The high quality single crystal samples obtained by this technique enable researchers to investigate the various electronic properties by different techniques.

Optical spectroscopy is a powerful bulk technique to investigate charge dynamics and band structure of materials as it probes both free carriers and interband excitations. Our previous studies of FeSe thin film on STO¹⁸ has shown some interesting results but it is not enough to understand the complex physics in FeSe. No spectral change associated with the structural or nematic order was observed due to the relatively low quality of the thick films. So further optical studies of bulk FeSe are necessary. In this work, we report an optical spectroscopy study on high quality FeSe single crystal.

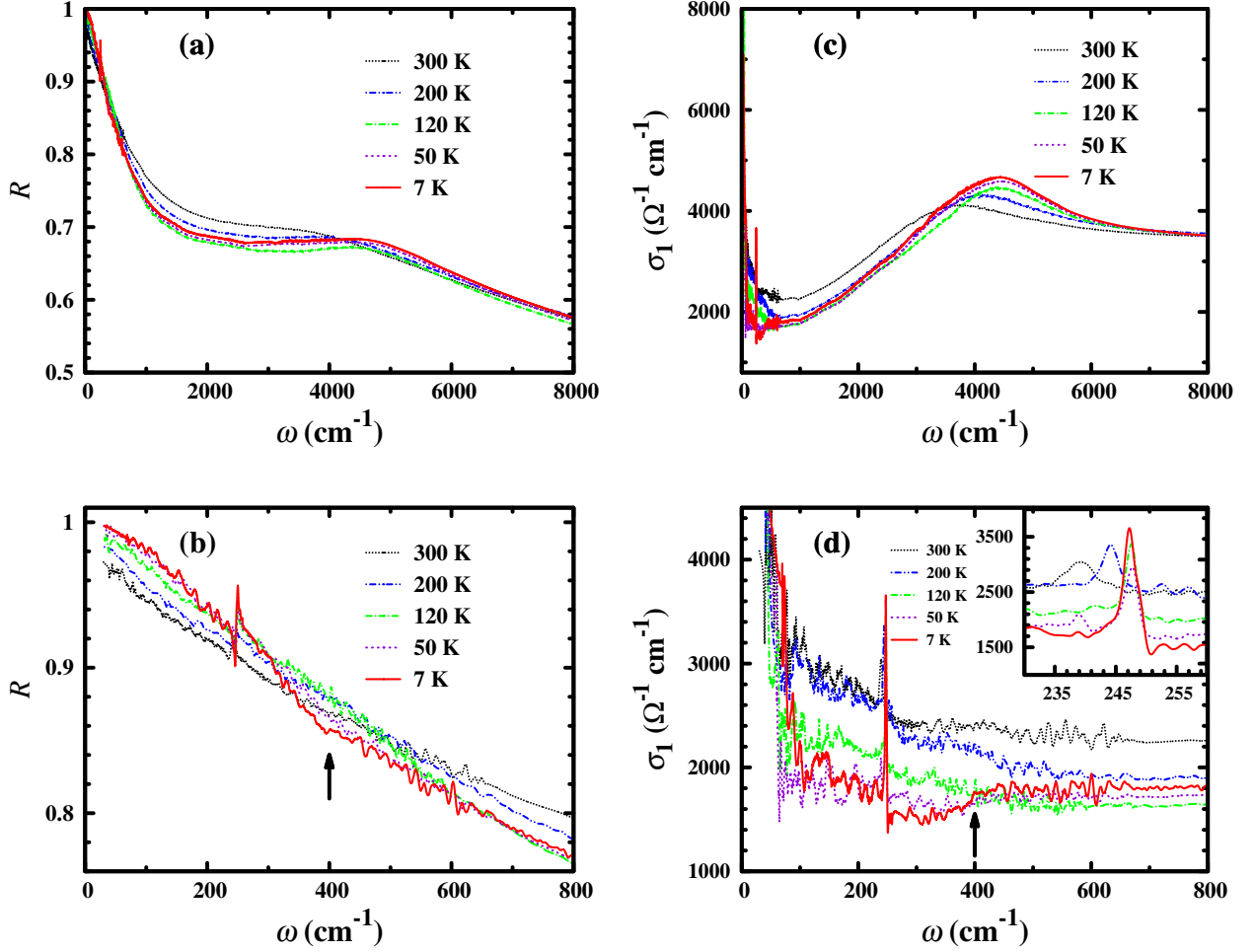


FIG. 1. (Color online) **a** Optical reflectivity at five representative temperatures in the frequency range from 0 to 8000 cm^{-1} . **b** Optical reflectivity from 0 to 800 cm^{-1} . The arrow marks the position of the suppression of $R(\omega)$ below 120 K. **c** Optical conductivity $\sigma_1(\omega)$ at five representative temperatures from 0 to 8000 cm^{-1} . **d** Optical conductivity $\sigma_1(\omega)$ from 0 to 800 cm^{-1} . The arrow marks the position of the gap-like peak below 120 K. Inset of (d) shows the phonon peaks in the expanded scale

II. EXPERIMENTAL

The FeSe single crystals were grown using vapor transport method¹⁷. The optical reflectance measurements were performed on a combination of Bruker IFS 80 v/s and 113 v spectrometers in the frequency range from 30 to 26000 cm^{-1} . An *in situ* gold and aluminum overcoating technique was used to get the reflectivity $R(\omega)$. The real part of conductivity $\sigma_1(\omega)$ was obtained by the Kramers-Kronig transformation of $R(\omega)$ employing an extrapolation method with X-ray atomic scattering functions¹⁹. This new method of Kramers-Kronig transformation was proved to be more accurate and effective in analyzing the optical reflectivity.

III. RESULTS AND DISCUSSIONS

The temperature-dependent in-plane optical reflectivity $R(\omega)$ and conductivity $\sigma_1(\omega)$ are shown in Fig. 1. At low frequencies (the lower panels of Fig. 1) a sharp phonon mode at about 240 cm^{-1} can be seen clearly. This mode shifts slightly to higher frequency and becomes sharper with decreasing temperature. It can be seen more clearly in the inset of Fig. 1d. This phonon mode is commonly seen in Fe-based superconductors and ascribed to the in-plane displacements of Fe-As(Se) atoms. The mode appears at a higher frequency than that observed at 187 cm^{-1} for $\text{Fe}_{1.03}\text{Te}$ and 204 cm^{-1} for $\text{FeTe}_{0.55}\text{Se}_{0.45}$ samples²⁰. The effect is due to the reduced mass of the Se atom as compared with the Te atom. The clear observation of this in-plane phonon mode and its temperature-dependent effect indicates the good quality of the single crystal sample.

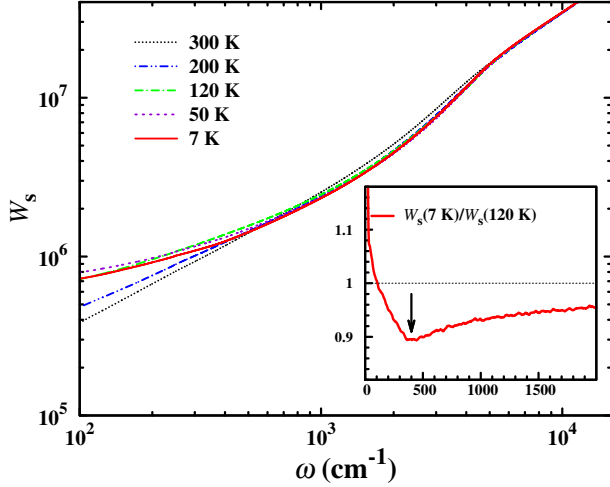


FIG. 2. (Color online) Cutoff frequency dependent spectral weight at five different temperatures. Inset: the normalized spectral weight $W_s(7\text{ K})/W_s(120\text{ K})$ up to 2000 cm^{-1}

Below the structural phase transition (in nematic phase) a clear temperature dependent suppression is seen in $R(\omega)$, leading to a dip-like feature near the frequency of 400 cm^{-1} as indicated by an arrow in Fig. 1b. Accordingly, $\sigma_1(\omega)$ shows a peak-like structure at somewhat higher frequency. This is a typical gap-like feature. Moreover, this feature can be seen from the spectral weight analysis as we shall present below (see inset of Fig. 2). ARPES studies have revealed that there exists the splitting of d_{xz} and d_{yz} bands and possible additional separation of $d_{xz/yz}$ and d_{xy} bands in nematic phase^{21–23}. The energy scale of the band splitting at low temperature is about 50 meV at M point^{21,22} and 30 meV at Γ point²³ which is comparable to the central energy of the Lorentz peak (540 cm^{-1} or 67 meV) observed on $\sigma_1(\omega)$ (see Table I and discussion below). The gap-like feature in our optical spectra thus should be associated with the band reconstruction below T_s . Note that in the optical-conductivity measurements the gap value should be less than the location of the peak in $\sigma_1(\omega)$, thus the discrepancy between the results from ARPES and optics is small. It is also worth noting that a previous pump-probe experiment on FeSe film indicated an emergence of gap-like quasiparticles (associated with a energy gap $\Delta \approx 36\text{ meV}$) below 100 K ²⁴ though the extraction of an energy gap from this technique is indirect. This gap-like feature is similar as the energy gap formation in nematic phase observed by infrared experiment in parent compounds of iron pnictides^{25–27} (including 122, 111, and 1111 systems). In these iron pnictides the nematicity is generally considered to be driven by magnetism²⁸. However, unlike the iron pnictides, there is no stripe-type long-range antiferromagnetic order in FeSe at any temperature. Because the absence of long-range magnetic order and weak spin-fluctuation at high temperature around T_s observed

by NMR¹¹ the orbital-driven model seem to be more plausible. This scenario was support by some ARPES experiments²¹ and some theoretical studies²⁹. However, a recent theoretical study based on J_1 - J_2 model of spin-1 local moments with strongly frustrated exchange interactions indicated that its quantum fluctuations can lead to a nematic quantum paramagnetic phase consistent with the observations in FeSe³⁰. A recent inelastic neutron scattering study¹² revealed substantial commensurate stripe spin fluctuations in the tetragonal phase and there exists strong coupling between the stripe spin fluctuations, nematicity and superconductivity in FeSe. A polarized ultrafast spectroscopy study was also in favor of the magnetic origin of nematicity³¹. Apparently, the nematicity which is responsible for the band reconstruction in FeSe have not yet well-understood. The gap-like feature observed in our optical results could give helpful information on this topic.

At low frequencies, Drude-like response exists in the conductivity spectrum (see Fig. 1d). This behavior is also observed in Fe-pnictides such as $\text{FeTe}_{0.55}\text{Se}_{0.45}$ and BaFe_2As_2 ^{25,26}. To estimate the Drude weight or plasma frequency of the FeSe and characterize the spectral change across the phase transition, we decompose the optical conductivity spectral into different components using a Drude-Lorentz analysis. The dielectric function has the form^{25,32–34}

$$\epsilon(\omega) = \epsilon_\infty - \sum_k \frac{\omega_{p,k}^2}{\omega^2 + i\omega/\tau_k} + \sum_j \frac{\Omega_j^2}{\omega_j^2 - \omega^2 - i\omega/\tau_j}, \quad (1)$$

where ϵ_∞ is the dielectric constant at high energy, the middle and last term are the Drude and Lorentz components. The complex conductivity is $\sigma(\omega) = \sigma_1(\omega) + i\sigma_2(\omega) = -\omega[\epsilon(\omega) - \epsilon_\infty]/4\pi$. We use two Drude components (a sharp one and a broaden one) and several Lorentz components, including a Lorentz peak of phonon, to fit the optical conductivity. The conductivity spectra at different temperatures can be reproduced. The fitting results at two representative temperatures, the lowest one at 7 K and the room temperature, are shown in Fig. 3. Detailed fitting parameters at low frequencies are listed in Table I. Here, a Lorentz component at low frequency is added to character the gap-opening like feature of $\sigma_1(\omega)$ but not used above T_s . Usually the energy of the gap can be estimated by the central frequency of this Lorentz model²⁵. In this case the central frequency is about 540 cm^{-1} (67 meV) at 7 K . In the two component approach, the overall plasma frequency ω_p could be considered as being contributed from two different channels and be calculated as $\omega_p = (\omega_{p1}^2 + \omega_{p2}^2)^{1/2}$. In the present case we obtain the $\omega_p \approx 10000\text{ cm}^{-1}$ above T_s and $\omega_p \approx 7200\text{ cm}^{-1}$ at low temperature as shown in Table I. Another method to estimate the overall plasma frequency is to calculate the low- ω spectral weight, $\omega_p^2 = 8 \int_0^{\omega_c} \sigma(\omega) d\omega$. The cut-off frequency ω_c is chosen so as to make the integration cover all contribution from free carriers and exclude contribution from interband transition. Usually,

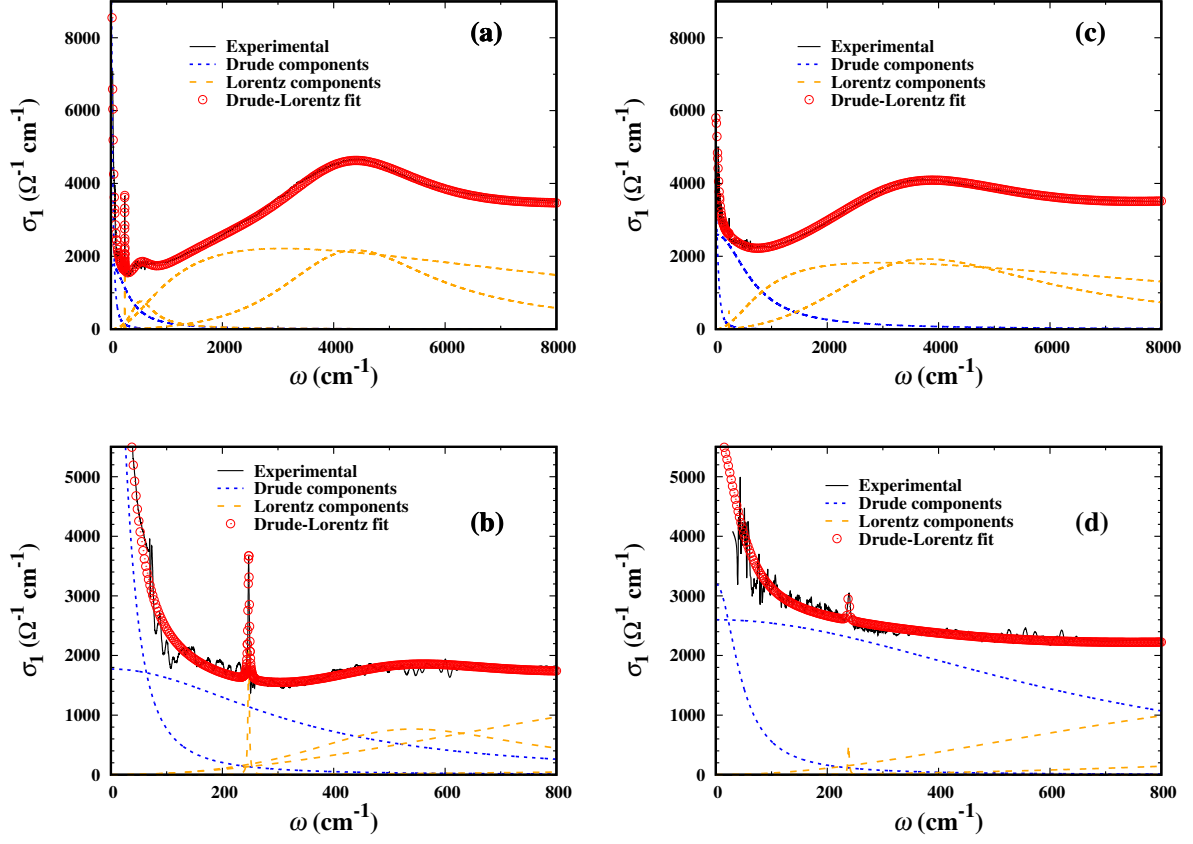


FIG. 3. (Color online) The experimental data of $\sigma_1(\omega)$ together with the Drude-Lorentz fits at 7 K (**a** from 0 to 8000 cm^{-1} , **b** from 0 to 800 cm^{-1}) and 300 K (**c** from 0 to 8000 cm^{-1} , **d** from 0 to 800 cm^{-1})

TABLE I. Parameters of Drude-Lorentz fit at low frequencies and the overall plasma frequencies at different temperatures

T (K)	Drude1		Drude2		Lorentz			ω_p	
	ω_{p1} (cm^{-1})	Γ_1 (cm^{-1})	ω_{p2} (cm^{-1})	Γ_2 (cm^{-1})	ω_0 (cm^{-1})	ω_p (cm^{-1})	Γ (cm^{-1})	$(\omega_{p1}^2 + \omega_{p2}^2)^{1/2}$ (cm^{-1})	$[8 \int_0^{\omega_c} \sigma(\omega) d\omega]^{1/2}$ (cm^{-1})
300	10200	670	3310	45	-	-	-	10700	8900
200	10000	655	3330	36	-	-	-	10500	8700
120	8800	640	3500	36	-	-	-	9400	8500
50	6300	409	3600	34	510	4600	600	7300	6570
7	5940	330	4160	30	540	4840	510	7200	6170

the integral goes to a frequency where the conductivity shows a minimum. By choosing ω_c (780 cm^{-1} at 300 K, 750 cm^{-1} at 200 K, 700 cm^{-1} at 120 K, 360 cm^{-1} at 50 K and 330 cm^{-1} at 7 K) we recalculate the plasma frequencies and the results are shown in Table I. All the values of ω_p obtained by the second method are smaller than the former ones. Because the balance of Drude tail and Lorentz onset can not be accurately determined by the minimum of conductivity, the difference between two methods is not unreasonable.

The overall plasma frequency is related to the carrier density n and effective mass m^* by $\omega_p^2 = ne^2/(\epsilon_0 m^*)$. Assuming that the effective mass of charge carriers does not change much with decreasing temperature, we get

the ratio of $\omega_{p,7K}^2/\omega_{p,300K}^2$ (45 % for first method and 48 % for second method), suggesting more than half of the free carrier spectral weight is suppressed after the structural or nematic phase transition. So the carrier density of FeSe at low temperature becomes significantly small. We remark that the band reconstruction or gap-like suppression below nematic phase transition was not observed in our earlier study on FeSe film grown on SrTiO_3 substrate by pulsed laser deposition technique¹⁸, most likely due to the relatively poor quality of the film compared with present single crystal samples grown by vapor transport technique. The significantly small ω_p at low temperature is consistent with very small Fermi energy ($\epsilon_F \lesssim 10$ meV) seen in recent ARPES and many

other measurements^{21–23,35,36}. In fact, due to the very small ε_F , it is suggested that FeSe is in the BEC-BCS crossover regime^{13,37} where $\Delta/\varepsilon_F \sim 1$.

As temperature decreases, from Fig. 1c we can clearly see that the broad peak at $4000 - 5000 \text{ cm}^{-1}$ becomes narrow and shifts to higher energy. By defining the spectral weight as $W_s = \int_0^\omega \sigma_1(\omega) d\omega$, the transfer of spectral weight can also be seen in Fig. 2. W_s at low temperature between 2000 and 4000 cm^{-1} is lower but recovers at higher frequency, *i. e.*, the spectral weight is transferred to higher frequency region. This feature in the present high quality FeSe single crystal is more prominent than that observed in FeSe film on STO substrate¹⁸ and even other iron pnictides^{38,39}. However, the relevant energy scale for FeSe is smaller than that for BaFe_2As_2 whose spectral weight was transferred to a region above 5000 cm^{-1} . Such temperature-induced spectral weight transfer was ascribed to the Hund's coupling effect between itinerant and localized Fe 3d electrons in different orbitals³⁸. FeSe as well as other iron-chalcogenide compounds have stronger electron correlation effect, leading to a larger local moment of $2\mu_B$ ⁴⁰ and higher band renormalization factor⁴¹. The relatively smaller energy scale of temperature-induced spectral weight transfer reflects the complex interplay effect between Hund's correlation effect and kinetic energy of electrons in those iron-based superconductors.

IV. SUMMARY

In summary, we perform an in-plane optical spectroscopy measurement on high quality FeSe single crystals grown by a vapor transport technique. Below the structural or nematic phase transition at 90 K, the reflectivity spectrum clearly shows a gradual suppression around 400 cm^{-1} and the conductivity spectrum shows a peak at higher frequency. The energy scale of this gap-like feature is comparable to the band splitting observed by ARPES and should be associated with the band reconstruction accompanied by the structural transition. The low-frequency conductivity consists of two Drude components and the overall plasma frequency is smaller than that of the FeAs based compounds. Further reduction of plasma frequency is observed below the structural phase transition temperature, being consistent with the very small Fermi energy observed in other measurements. Similar to iron pnictides, a temperature-induced spectral weight transfer is observed for FeSe, providing evidence for the strong correlation effect.

ACKNOWLEDGMENTS

This work was supported by the National Natural Science Foundation of China (11120101003, 11327806), and the National Basic Research Program of China (2012CB821403).

Conflict of interest

The authors declare that they have no conflict of interest.

* nlwang@pku.edu.cn

¹ Medvedev S, McQueen TM, Troyan IA et al (2009) Electronic and magnetic phase diagram of $\beta\text{-Fe}_{1.01}\text{Se}$ with superconductivity at 36.7 K under pressure. *Nat Mater* 8:630–633

² Lu XF, Wang NZ, Wu H et al (2015) Coexistence of superconductivity and antiferromagnetism in $(\text{Li}_{0.8}\text{Fe}_{0.2})\text{OHFeSe}$. *Nat Mater* 14:325–329

³ Lin H, Xing J, Zhu XY et al (2016) Robust superconductivity and transport properties in $(\text{Li}_{1-x}\text{Fe}_x)\text{OHFeSe}$ single crystals. *Sci China-Phys Mech Astron* 59:657404

⁴ Liu DF, Zhang WH, Mou DX et al (2012) Electronic origin of high-temperature superconductivity in single-layer FeSe superconductor. *Nat Commun* 3:931

⁵ He SL, He JF, Zhang WH et al (2013) Phase diagram and electronic indication of high-temperature superconductivity at 65 K in single-layer FeSe films. *Nat Mater* 12:605–610

⁶ Tan SY, Zhang Y, Xia M et al (2013) Interface-induced superconductivity and strain-dependent spin density waves in FeSe/SrTiO₃ thin films. *Nat Mater* 12:634–640

⁷ Lee JJ, Schmitt FT, Moore RG et al (2014) Interfacial mode coupling as the origin of the enhancement of T_c in FeSe films on SrTiO₃. *Nature* 515:245–248

⁸ Zhang ZC, Wang YH, Song Q et al (2015) Onset of the

Meissner effect at 65 K in FeSe thin film grown on Nb-doped SrTiO₃ substrate. *Sci Bull* 60:1301–1304

⁹ Jia JF (2015) Superconductivity at 65 K in monolayer FeSe by ex situ Meissner effect measurement. *Sci Bull* 60:1368–1369

¹⁰ Ge JF, Liu ZL, Liu CH et al (2015) Superconductivity above 100 K in single-layer FeSe films on doped SrTiO₃. *Nat Mater* 14:285–289

¹¹ Baek SH, Efremov DV, Ok JM et al (2014) Orbital-driven nematicity in FeSe. *Nat Mater* 14:210–214

¹² Wang QS, Shen Y, Pan BY et al (2016) Strong interplay between stripe spin fluctuations, nematicity and superconductivity in FeSe. *Nat Mater* 15:159–163

¹³ Kasahara S, Watashigea ST, Hanagurib T et al (2014) Field-induced superconducting phase of FeSe in the BCS-BEC cross-over. *Proc Natl Acad Sci USA* 111:16309–16313

¹⁴ Tan SY, Fang Y, Xie DH et al (2016) Observation of Dirac cone band dispersions in FeSe thin films by photoemission spectroscopy. *Phys Rev B* 93:14513

¹⁵ Wu XX, Liang Y, Fan H et al (2016) Nematic orders and nematicity-driven topological phase transition in FeSe. *arXiv:1603.02055*

¹⁶ Hu RW, Lei HC, Abeykoon M et al (2011) Synthesis, crystal structure, and magnetism of $\beta\text{-Fe}_{1.00(2)}\text{Se}_{1.00(3)}$ single

- crystals. Phys Rev B 83:224502
- ¹⁷ Böhmer AE, Hardy F, Eilers F et al (2013) Lack of coupling between superconductivity and orthorhombic distortion in stoichiometric single-crystalline FeSe. Phys Rev B 87:180505
 - ¹⁸ Yuan RH, Kong WD, Yan L et al (2013) In-plane optical spectroscopy study on FeSe epitaxial thin film grown on SrTiO₃ substrate. Phys Rev B 87:144517
 - ¹⁹ Tanner DB (2015) Use of X-ray scattering functions in Kramers-Kronig analysis of reflectance. Phys Rev B 91:035123
 - ²⁰ Homes CC, Akrap A, Wen JS et al (2010) Electronic correlations and unusual superconducting response in the optical properties of the iron chalcogenide FeTe_{0.55}Se_{0.45}. Phys Rev B 81:180508(R)
 - ²¹ Nakayama K, Miyata Y, Phan GN et al (2014) Reconstruction of band structure induced by electronic nematicity in an FeSe superconductor. Phys Rev Lett 113:237001
 - ²² Chubukov AV, Fernandes RM, Schmalian J (2015) Origin of nematic order in FeSe. Phys Rev B 91:201105
 - ²³ Zhang P, Qian T, Richard P et al (2015) Observation of two distinct d_{xz}/d_{yz} band splittings in FeSe. Phys Rev B 91:214503
 - ²⁴ Wen YC, Wang KJ, Chang HH et al (2012) Gap opening and orbital modification of superconducting FeSe above the structural distortion. Phys Rev Lett 108:267002
 - ²⁵ Hu WZ, Dong J, Li G et al (2008) Origin of the spin density wave instability in AFe₂As₂ (A=Ba,Sr) as revealed by optical spectroscopy. Phys Rev Lett 101:257005
 - ²⁶ Hu WZ, Li G, Zheng P et al (2009) Optical study of the spin-density-wave properties of single-crystalline Na_{1- δ} FeAs. Phys Rev B 80:100507
 - ²⁷ Dong T, Chen ZG, Yuan RH et al (2010) Formation of partial energy gap below the structural phase transition and the rare-earth element-substitution effect on infrared phonons in ReFeAsO (Re=La, Nd, and Sm). Phys Rev B 82:054522
 - ²⁸ Fernandes RM, Chubukov AV, Schmalian J (2014) What drives nematic order in iron-based superconductors? Nat Phys 10:97–104
 - ²⁹ Mukherjee S, Kreisel A, Hirschfeld PJ et al (2015) Model of electronic structure and superconductivity in orbitally ordered FeSe. Phys Rev Lett 115:026402
 - ³⁰ Wang F, Kivelson SA, Lee DH (2015) Nematicity and quantum paramagnetism in FeSe. Nat Phys 11:959–963
 - ³¹ Luo CW, Cheng PC, Wang SH et al (2016) Unveiling the hidden nematicity and spin subsystem in FeSe. arXiv:1603.08710
 - ³² Nakajima M, Ishida S, Kihou K et al (2010) Evolution of the optical spectrum with doping in Ba(Fe_{1- x} Co _{x})₂As₂. Phys Rev B 81:104528
 - ³³ Wu D, Barišić N, Kallina P et al (2010) Optical investigations of the normal and superconducting states reveal two electronic subsystems in iron pnictides. Phys Rev B 81:100512(R)
 - ³⁴ Tu JJ, Li J, Liu W et al (2010) Optical properties of the iron arsenic superconductor BaFe_{1.85}Co_{0.15}As₂. Phys Rev B 82:174509
 - ³⁵ Terashima T, Kikugawa N, Kiswandhi A et al (2014) Anomalous Fermi surface in FeSe seen by Shubnikov-de Haas oscillation measurements. Phys Rev B 90:144517
 - ³⁶ Audouard A, Duc F, Drigo L et al (2015) Quantum oscillations and upper critical magnetic field of the iron-based superconductor FeSe. Europhys Lett 109:27003
 - ³⁷ Lubashevsky Y, Lahoud E, Chashka K et al (2012) Shallow pockets and very strong coupling superconductivity in FeSe _{x} Te_{1- x} . Nat Phys 8:309–312
 - ³⁸ Wang NL, Hu WZ, Chen ZG et al (2012) High energy pseudogap and its evolution with doping in Fe-based superconductors as revealed by optical spectroscopy. J Phys Condens Matter 24:294202
 - ³⁹ Schafgans AA, Moon SJ, Pursley BC et al (2012) Electronic correlations and unconventional spectral weight transfer in the high-temperature pnictide BaFe_{2- x} Co _{x} As₂ superconductor using infrared spectroscopy. Phys Rev Lett 108:147002
 - ⁴⁰ Gretarsson H, Lupascu A, Kim J et al (2011) Revealing the dual nature of magnetism in iron pnictides and iron chalcogenides using X-ray emission spectroscopy. Phys Rev B 84:100509(R)
 - ⁴¹ Maletz J, Zabolotnyy VB, Evtushinsky DV et al (2014) Unusual band renormalization in the simplest iron-based superconductor FeSe_{1- x} . Phys Rev B 89:220506(R)